2008

A cylindrical silicon-on-insulator microdosimeter: charge collection characteristics

Amy Ziebell
University of Wollongong, alz97@uow.edu.au

Wee Han Lim
University of New South Wales

Mark I. Reinhard
Australian Nuclear Science and Technology Organisation

Iwan Cornelius
University of Wollongong, iwan@uow.edu.au

Dale A. Prokopovich
Australian Nuclear Science and Technology Organisation, dap11@uow.edu.au

See next page for additional authors

A Cylindrical Silicon-on-Insulator Microdosimeter: Charge Collection Characteristics

A. L. Ziebell, *Student Member, IEEE*, W. H. Lim, *Student Member, IEEE*, M. I. Reinhard, *Member, IEEE*, I. Cornelius, *Member, IEEE*, D. A. Prokopovich, *Student Member, IEEE*, R. Siegele, A. S. Dzurak, *Member, IEEE*, and A. B. Rosenfeld, *Senior Member, IEEE*

***Abstract*—A novel silicon-on-insulator microdosimeter for estimating the radiobiological effectiveness (RBE) of a mixed radiation field is presented. An ion beam induced charge collection study has confirmed the microdosimeter possesses well defined micron sized 3D cylindrical sensitive volumes. An array of these SVs has the capability of studying the track structure of high energy heavy ions typical of a deep space environment.**

***Index Terms*—Ion beams, microdosimetry, radiobiological effectiveness, silicon-on-insulator.**

I. Introduction

An effective way to determine the radiobiological effectiveness (RBE) of a mixed radiation field is to employ the regional microdosimetry approach [1]. This approach has been applied to: fast neutron and charged particle radiation therapy [2]–[7], predicting single event upsets (SEUs) in micro and nano electronics [8], and assessing the biological risk posed to radiation workers, high altitude and space aviation crew [9], [10]. The microdosimetry approach has the advantage that no prior knowledge of the particles contained within the field is required. The radiobiological properties of the field are inferred by measuring the spectral distribution of stochastic lineal energy events $f(y)$ in a micron sized site, where y is the quotient of energy deposited by a single event ε, and the volume's mean chord length $\overline{\ell}$ i.e., $\varepsilon/\overline{\ell}$ for all primary and secondary particles generated during the exposure of the tissue or electronics to ionizing radiation. With knowledge of $f(y)$ the RBE is calculated using $\int Q(y)y^2 f(y)d(\log y)$, where $Q(y)$ is a quality factor obtained from radiobiological experiments [1], [2]. Experimental measurements of $f(y)$ require a radiation detection instrument with a sensitive volume (SV) equivalent in size to that of a biological cell. Traditionally gas proportional counters have been used. Such instruments have the advantage of excellent tissue equivalency of the gas but suffer from some well documented shortcomings. These shortcomings include: wall effects, a large physical volume and the need for a high operating voltage [1], [11]–[14]. At present there exists a need for an easy to use portable microdosimeter with improved spatial resolution. Solid-state detectors address this need.

The first comparison of a single *p-n* junction silicon solid-state detector to a gas proportional counter was made in 1980 [15]. The spectra from the silicon solid-state detector showed significant differences to that obtained from the gas proportional counter. This was mainly due to the silicon's larger than ideal sensitive thickness. Since that first comparison the research and development of solid-state microdosimeters has progressed markedly.

In the 1990's an array of reverse-biased silicon *p-n* junctions was proposed for characterizing complex radiation environments inside spacecraft and aircraft [16], [17]. The work was intended to have applications in determining single event upset (SEU) risks to microelectronics and as a biological microdosimeter for personnel monitoring. The detector was used for the separation of neutron irradiation in a mixed radiation field. It was based on the deposition of energy by secondary charged particles originating in silicon. Microdosimetric spectra obtained from the device have not been presented and the response of the detector was qualitative only.

A solid-state Ultraviolet erasable Programmable Read Only Memory (UVPROM) device has also been developed for monitoring the exposure of systems to ionizing radiation [18]. This device consists of an array of Floating gate Avalanche injection Metal Oxide Semiconductor (FAMOS) transistors. The application of the floating gate as a dosimeter is based on measuring the gradual neutralization of charge, hence subsequent change in transistor logic state, by ionizing radiation and associating this change to cell deactivation in a mixed radiation field. Considering the size of the polysilicon gate is of nanometer order, this devices may be considered as the first approach to solid state nanodosimetry

Recently a monolithic $\Delta E - E$ silicon telescope has been introduced as a possible microdosimeter [19]. Operated solely, the ΔE stage of the device can be employed as a planar microdosimeter for fields normal to the surface. With both stages operated in co-incidence the device may be used to discern the

Manuscript received April 17, 2008; revised July 30, 2008. Current version published December 31, 2008. This work was supported in part by the Australian Research Council Discovery Project Grant N 0663785, the Australian Nuclear Science and Technology Organisation (ANSTO) Heavy Ion Microprobe staff, the Australian Research Council (ARC) Discovery Project Grant N 0663785, and the Australian Institute of Nuclear Science and Engineering (AINSE).

A. L. Ziebell, I. Cornelius, and A. B. Rosenfeld are with the Centre for Medical Radiation Physics, University of Wollongong, North Wollongong, NSW 2522, Australia (e-mail: alz97@uow.edu.au; ic02@uow.edu.au; anatoly@uow.edu.au).

W. H. Lim and A. S. Dzurak are with the School of Electrical Engineering and Telecommunications, University of New South Wales, Sydney, NSW 2052, Australia (e-mail: z3087021@student.unsw.edu.au; a.dzurak@unsw.edu.au).

M. I. Reinhard and D. A. Prokopovich are with the Australian Nuclear Science and Technology Organisation, Lucas Heights, NSW 2234, Australia (e-mail: mrz@ansto.gov.au; dpr@ansto.gov.au).

Color versions of one or more of the figures in this paper are available online at http://ieeexplore.ieee.org.

Digital Object Identifier 10.1109/TNS.2008.2004464

identity of an incident particle (given that the range of the particle is less than the thickness of the device) and assess the RBE of the field.

The concept of obtaining tissue equivalent microdosimetric measurements using a solid state detector was first introduced by Rosenfeld [20]. This approach uses a planar 2D semiconductor-on-insulator (SOI) based device developed at the Centre for Medical Radiation Physics (CMRP), University of Wollongong, Australia [21].

This device consists of a 2D array of rectangular parallelepiped diode structures all within close proximity to one another. Each SV is 10 μm thick and has a surface area of 30×30 μm^2. All SVs are connected in parallel.

The device has the potential for application in the prediction of Single Event Upsets (SEUs) in silicon microelectronics. SEUs occur when a charged particle, such as a recoil ion produced from a high energy neutron or proton interaction, deposits some critical amount of charge in the *p-n* junction of a microelectronic device. Since it is silicon based, the SOI microdosimeter is capable of monitoring and modelling this energy deposition. This is relevant to both medical and radiation protection devices where atmospheric neutrons have been observed to induce SEUs in medical implantable devices such as pacemakers as well as automotive electronics and the safeguard instrumentation used in reactor facilities [22]–[24]. Previous work has investigated the response of the SOI microdosimeter to neutrons [25], [26] and heavy ions [27]. The device has also been successfully tested for applications in radiation therapy [28], radiation protection [10], [29], and deep space environments at the NASA radiation facility, Brookhaven National Laboratory (BNL) [9] with 0.6 GeV/n iron and 1.0 GeV/n titanium ions.

Studies on the charge collection characteristics of the device have found that due to the electric field distribution within the planar SV, the charge collection efficiency (CCE) of the device varies with position [30]. This introduces significant lateral charge diffusion effects which complicate charge collection. The elongated rectangular geometry of the SV also gives rise to a less than ideal chord length variance that can lead to an over-estimation of energy deposited within the SV. A cube or cylinder is known to provide a better approximation to the ideal geometry of the sphere whilst still providing a realistic geometry for successful fabrication utilising the semiconductor planar process [12].

Based on a decade of experience a new generation SOI microdosimeter has been proposed by the CMRP and developed in collaboration with the Australian Nuclear Science and Technology Organisation (ANSTO) and the University of New South Wales (UNSW). The design of this new device is based on an array of physically isolated 3D cylindrical *p-i-n* diode SVs. The cylindrical geometry reduces the chord length variance throughout the SV and supports a radial electric field. The radial electric field facilitates the collection of all deposited charge via drift allowing for a near 100% CCE across the entire SV. Fig. 1 shows a schematic of the SV design and the $1/r$ electrical field distribution. Each of these SVs is designed as part of a raised mesa structure to further isolate the SV from any unwanted charge collection effects.

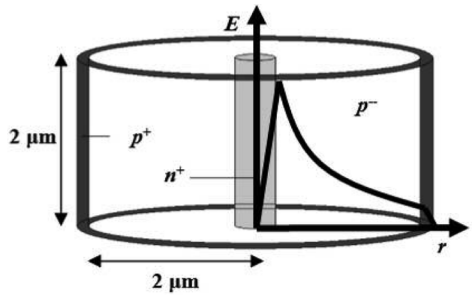

Fig. 1. A schematic showing the design of a 3D cylindrical SOI microdosimeter diode. The design overcomes the shortcomings of the previous 2D planar SOI microdosimeter.

The array was designed to have translational symmetry. The symmetry being such that any single SV is surrounded by 4 identical SVs all connected in parallel to a separate read out channel. This dual channel read out gives the device: 1) the ability to correctly record the amount of energy an oblique charged particle deposits in individual adjacent SVs, and 2) the potential to differentiate between particles that possess the same unrestricted LET but produce different delta electron track structures which are associated with different quality factors. This potential for particle differentiation is particularly important for the characterization of high energy galactic cosmic rays (GCR). For example, within the GCR Fe ions with an energy of 1 GeV/u, and secondary alpha particles with an energy in the MeV range, possess the same unrestricted LET of about 200 keV/μm but produce distinctly different biological effects due to the different quality of each radiation. To differentiate between the two particles consideration of the different delta electron track structure that each produces must then be made. Fe ions produce delta electrons with a range of more than 10 μm. Therefore they could be detected by coincidence measurements of neighboring SVs in the array if the distance between each SV, d, was of the order of 5–15 μm. Such distances may be achieved with the planned implementation of 0.18 μm feature fabrication technology. For the prototype array presented, d is 80 μm (with the current fabrication technology allowing a minimum d of 10 μm). Fig. 2 shows the layout of this SV array design.

The purpose of this work was to examine the charge collection characteristics in SVs of this new SOI design, through the use of the ion beam induced charge collection (IBIC) technique, to: 1) confirm that each individual SV is a well defined 3D cylindrical site, and 2) confirm that an array of such SVs can be succesfully read out in a parallel mode. The electrical characteristics of this new SOI design are also presented.

II. The Device and Experimental Method

A. Fabrication

Fabrication of the SV employed planar processing techniques on a high resistivity (> 10 k$\Omega \cdot$ cm) p^{--} silicon on insulator (SOI) bonded wafer. Phosphorus and boron were diffused into the silicon wafer to produce the co-axial *p-i-n* diode structures. An etching process created the $\sim$2 μm thick, t, raised mesa SV

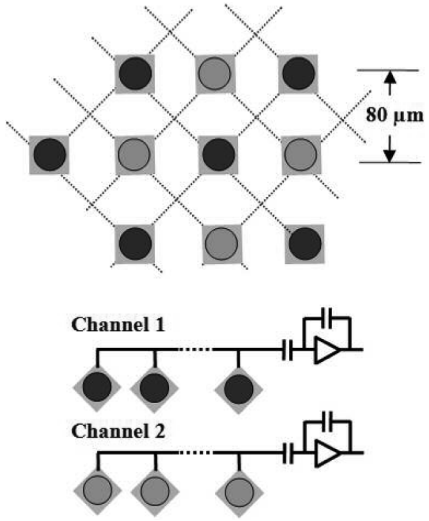

Fig. 2. A schematic of the design of the array of SVs. Notice that each SV is surrounded by 4 identical SVs all connected to a separate charge sensitive pre-amplifier.

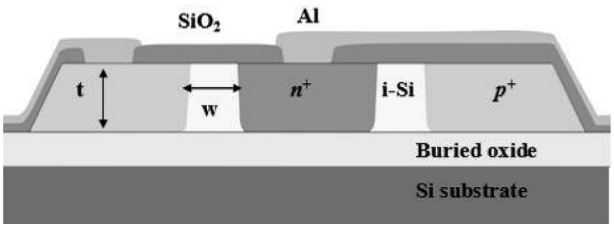

Fig. 3. A cross sectional schematic of the microdosimeter. Note the cylindrical nature of the design.

structures. 0.6 μm thick evaporated Al tracks were laid to facilitate electrical connection. A schematic of the SV is shown in Fig. 3. The annular p^{--} intrinsic region has a variable radial width, w. Further details on the fabrication and TCAD modelling of the device are presented in [31].

For this study three types of devices were fabricated for testing: 1) an independently read out SV of $w = 2$ μm, 2) an independently read out SV of $w = 10$ μm, and 3) a partial array of identical SVs, with $w = 2$ μm, all connected in parallel for single channel read out.

B. Electrical Characterisation

The electrical properties of each device was determined using conventional current-voltage (IV) and capacitance-voltage (CV) testing with a Keithley 6517A electrometer and a Boonton 7200 capacitance bridge. All measurements were performed under vacuum and at room temperature to allow for reproducible conditions.

C. Charge Collection Imaging

The charge collection characteristics of each device were experimentally determined via an IBIC study. This was performed using the Australian Nuclear Science and Technology Organisation (ANSTO) heavy ion microprobe. The use of this technique for characterizing silicon microdosimeter devices has previously been described in detail [32]. A mono-energetic beam of He ions focused to a diameter of approximately 1.0 μm was made incident on the microdosimeter device. The amount of energy deposited within the microdosimeter for each ion traversal, ΔE, was measured with a standard charge sensitive preamplifier, shaping amplifier and multi-channel analyser (MCA) in coincidence with digitized voltage signals of the beam position, x and y for each event in ΔE. Data triplets $(x, y, \Delta E)$ were saved for each event in a list mode file. Analysis software used these files to generate IBIC imaging maps displaying either; a spatially resolved image of the median amount of charge collected, a *median energy map*, or the spatially resolved frequency of events contained within a particular range of deposited energies of interest, a *frequency distribution map*, as a function of beam position

III. Results and Discussion

A. Electrical Characterisation

The typical reverse current and capacitance values for a functioning independently read out 2 or 10 μm width diode at a 9 V operating bias was 2–3 pA and 25 pF respectively. The typical reverse current for a functioning individual row on an arrayed device was 2 pA. The capacitance of the device with 6 functioning rows externally connected in parallel was 11 pF.

B. Charge Collection Imaging: 2 μm SV

The deposited energy from an independently read out 2 μm radial width SV reverse biased to 9 V in response to 3 MeV He ions is shown in Fig. 4(a). A peak can be seen at an energy of approximately 313 keV. The expected energy loss of a 3 MeV He ion in 2 μm of silicon is 392 keV (lineal energy transfer $(\mathrm{LET}) = 196$ keV/μm [33]). This suggests the thickness of the silicon superficial layer of the SOI wafer was in fact 1.6 μm. rather than the anticipated 2 μm. Such a variation in thickness can not be discounted as a result of the fabrication process. To understand the spatially resolved response of the diode to the 3 MeV He ion strikes the IBIC median energy map is shown in Fig. 4(b). As previously mentioned, the median energy map displays the median amount of charge collected by the charge sensitive preamplifier as a function of beam position (x, y). An orange (/light grey), red (/mid grey), or blue (/dark grey) pixel corresponds to a position on the SV where there is high, intermediate, or low median charge collection respectively. In Fig. 4(b) an annular region of high charge collection, orange (/light grey) pixels, can be seen. This shows an excellent spatial correlation to the SV's intrinsic (high resistivity p^{--} region). In this region all the deposited charge is expected to be collected under drift due to the presence of the strong electric field throughout the whole SV. The median energy map confirms this. The uniformity in the amount of charge collected in this region also implies a uniform thickness of the SV in the intrinsic region. Again referring to Fig. 4(b), regions of low charge collection, blue (/dark grey) pixels, can be seen in the centre and outer circumference of the SV. These regions correlate with the n^+ and p^+ doped regions of the SV respectively. High doping concentrations in these regions do not allow any penetration of the electric field. As such a statistically insignificant amount of charge is collected from the ions incident here due to a high degree of charge carrier recombination and reliance on charge diffusion in the absence of

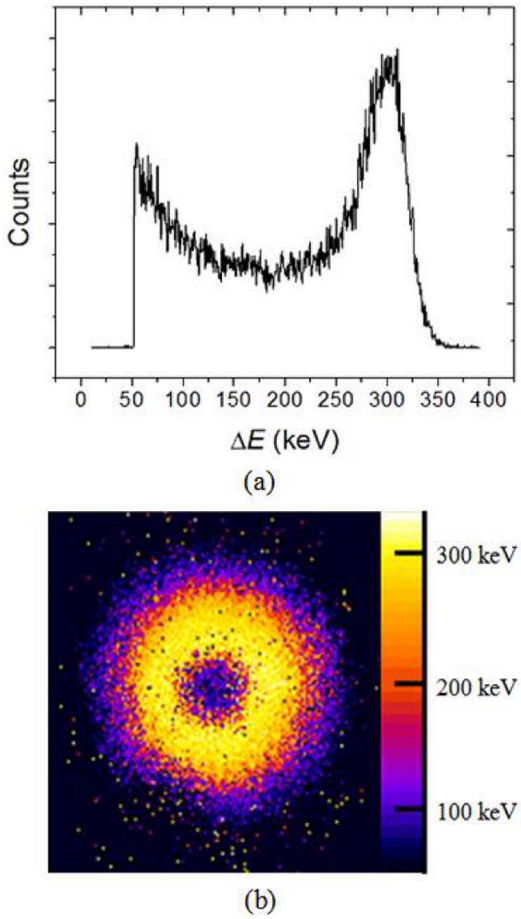

Fig. 4. (a) The energy spectrum produced by an independent 9 V reverse biased 2 μm radial width SV in response to a beam of 3 MeV He^{2+} ions. The peak is at an energy of ~ 300 keV suggesting the thickness of the SV is 1.6 μm rather than the expected 2 μm. (b) An IBIC median energy map of an independently read out 9 V reverse biased 2 μm radial width 3D cylindrical SV in response to a beam of 3 MeV He ions. A well defined annular region of full charge collection is observed as expected. A small amount of incomplete charge collection is observed around this annular region.

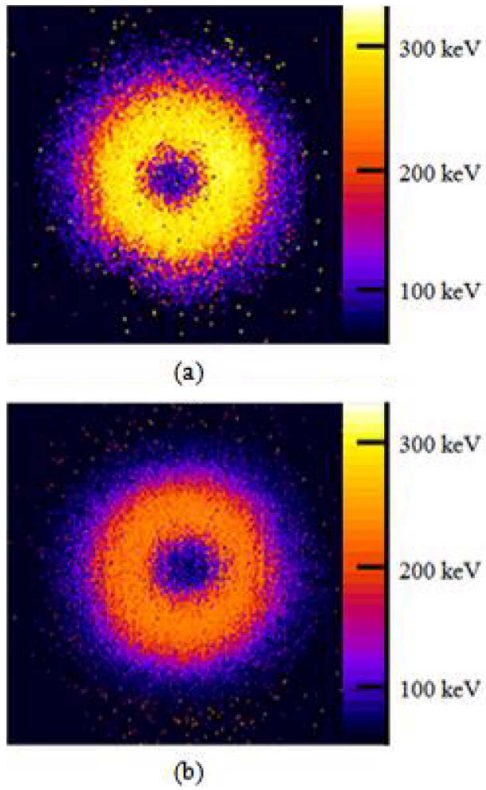

Fig. 5. An IBIC median energy map comparison of (a) an independently read out grounded 2 μm radial width SV in response to a beam of 3 MeV He ions and (b) an identical grounded SV in response to a beam of 5.5 MeV He ions. The geometrical response of the SV is consistent in both cases. In response to the 5.5 MeV there is a reduction in the amount of energy collected from each ion strike in accordance with the lower LET of the ions.

an applied electric field. At the outer and inner fringes of the annular high charge collection region, red (/mid grey) pixels indicate a level of intermediate charge collection. From Fig. 5 it can be seen that this incomplete charge collection is only statistically significant within less than 1 μm of the intrinsic region. No real events were observed in the regions external to the mesa structure of the SV. The sputtered events that can be seen are artefacts produced by ions which were initially directed towards their displayed location but were later made incident onto the SV of the microdosimeter due to scattering with the residual atoms and molecules within the evacuated beam tube.

Fig. 5(a) and (b) show the median energy maps of a grounded 2 μm radial width SV in response to a beam of 3 MeV He ions and a beam of 5.5 MeV He ions ($\mathrm{LET} = 135$ keV/μm) [15], respectively. In response to the more energetic, lower LET, 5.5 MeV ions the SV shows the same spatially resolved response as it does to the 3 MeV He ions. A comparison of the two deposited energy spectra corresponding to these median energy maps is shown in Fig. 6. Theoretical calculations considering the different LET of the two beams and the 1.6 μm thickness of the SV estimate a 96 keV difference in the energy the two beams will deposit within the SV. A 97 keV $\pm$ 6 keV difference was experimentally observed. This confirms the signal produced by the device is directly related to the LET of the incident ion as desired for any microdosimeter.

These results clearly demonstrate the fabricated SV has excellent charge collection characteristics even in passive mode (without bias). This is important for space applications of the device.

C. Charge Collection Imaging: 10 μm SV

The deposited energy spectrum from an independently read out 10 μm radial width grounded SV in response to 3 MeV He^{2+} ions is shown in Fig. 7. A peak can be seen at an energy of approximately 280 keV $\pm$ 3 keV. On the right of this peak a low statistics region of enhanced charge collection is observed. To understand the source of this enhanced charge collection IBIC frequency distribution maps were generated to examine the spatial origin of events contributing to the following regions of the energy spectrum: a) 60–235 keV, b) 250–300 keV and c) 310–350 keV. These regions correspond to the regions of the spectrum below the main peak, the peak itself, and the region of enhanced charge collection. The respective frequency distribution maps are shown in Fig. 8(a)–(c). From Fig. 8(a) it can be seen that counts below the main peak of the spectrum originated from ions incident upon the centre and outer fringes of the SV. From Fig. 8(b) it can be seen that counts in the main

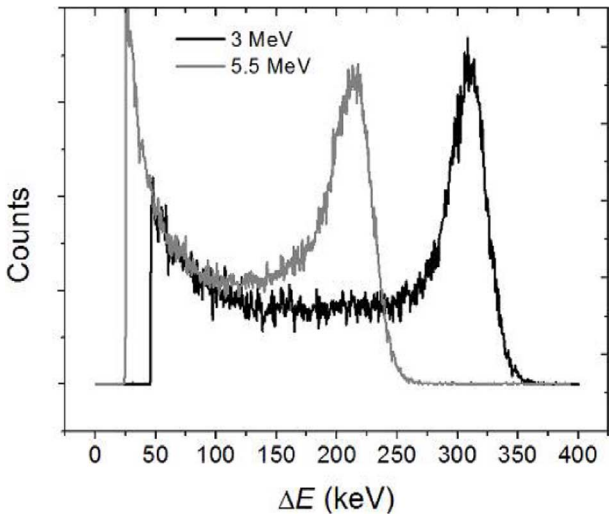

Fig. 6. A comparison of the two spectra produced by a grounded independently read out 2 μm radial width SV in response to a beam of 3 MeV He ions and a beam of 5.5 MeV He ions, respectively. There is a $97\ \mathrm{keV} \pm 6\ \mathrm{keV}$ difference in the amount of energy each beam deposited within the SV. This is in excellent agreement with 96 keV difference expected given the different LET of the two beams and the 1.6 μm thickness of the SV.

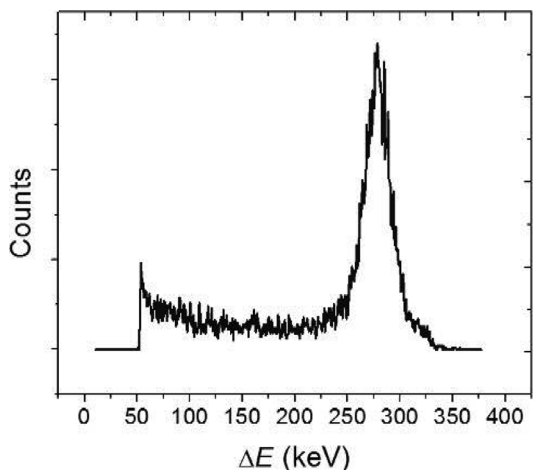

Fig. 7. The energy spectrum produced by a grounded independent 10 μm radial width SV in response to a beam of 3 MeV He^{2+} ions. There is a region of increased charge collection to the right of the main peak that was not seen in the spectrum produced by the 2 μm radial width independent SV.

peak of the spectrum originated from ions incident upon the annular intrinsic region of the SV. Counts in the main peak of the spectrum and below are therefore the result of the physical processes previously observed and discussed for the 2 μm radial width SV. The origin of counts above the main peak of the spectrum, those not previously seen in the study of the 2 μm radial width SV, is shown in Fig. 8(c). It can be seen that counts contributing to this region of increased charge collection originated from ions incident upon a region of the SV lying beneath the evaporated Al contact [see Fig. 8(d)]. Ions incident upon this part of the SV have an increased LET due to their prior attenuation through the Al. A calculation using [15] has shown this increased LET corresponds to the ions depositing approximately 10.1 keV more energy within the SV than those ions that did

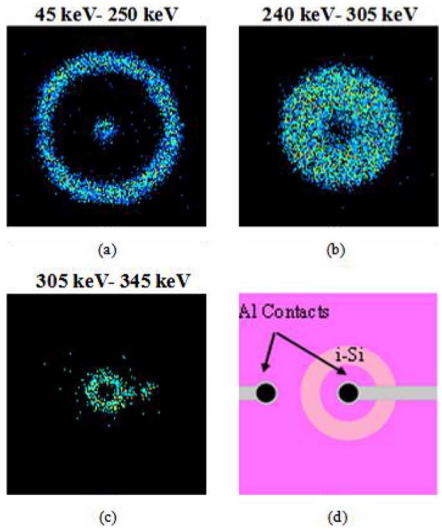

Fig. 8. (a)–(c) Event frequency distribution maps corresponding to the 3 distinct regions of the energy spectrum of. (d) A top view schematic of the Al tracks overlaying the SV. The increased charge collection observed in the energy spectrum appears to originate from ions incident upon the region of the SV lying directly beneath the overlaying Al track.

not undergo any attenuation. Such an increase in deposited energy is not sufficient to explain the observed region of enhanced charge collection. This 10 keV increase in energy would not be resolved from the main peak given the straggling of ions and the inherent 5 keV FWHM noise of the detector. A more likely source of the increased charge collection region is that the thickness of the silicon under the Al contact is slightly greater than that of the surrounding areas, a result of the fabrication process.

Even though the number of counts that result from the thicker region of the SV are low, it may lead to some inaccuracy in the final microdosimetric spectra. Reasons for the charge enhancement effect in this region of the SV should thus be investigated further.

D. Charge Collection Imaging: Array of 2 μm Svs

A partial arrayed device with 6 functioning rows of individual SVs was fabricated and demonstrated to be functional. Alternate rows, like those corresponding to *Channel 1* in Fig. 2, were connected in parallel to a single charge sensitive preamplifier and reverse biased to 10 V. The interlaying rows, like those corresponding to *Channel 2* in Fig. 2, were then connected in parallel and grounded.

A section of the device approximately $230 \times 230\ \mu\mathrm{m}^2$ in area was scanned with 3 MeV He^{2+} ions. The scan covered four SVs from two adjacent biased rows. Fig. 9 is a median energy map of this scan. The four connected SVs are observed to act as independent, well defined sites of complete charge collection as desired. No cross-talk between SVs was observed. This confirms the feasibility of producing a full array of independent cylindrical SVs.

A more detailed investigation into the charge collection characteristics of the array has revealed some peculiarities. These are reflected in Fig. 10; a comparison of the deposited energy spectrum of the $230 \times 230\ \mu\mathrm{m}^2$ section of the array and the deposited energy spectrum of the individual 2 μm radial width SV

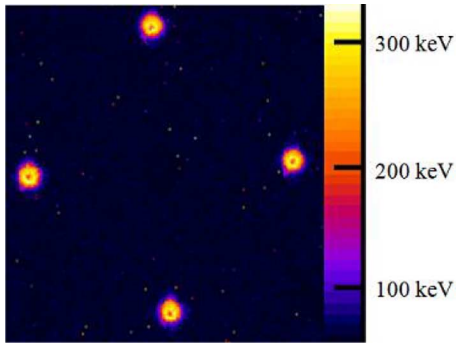

Fig. 9. An IBIC median energy map of a section of the 10 V reverse biased array. The four connected diodes can be seen to act as independent well defined sites of full charge collection.

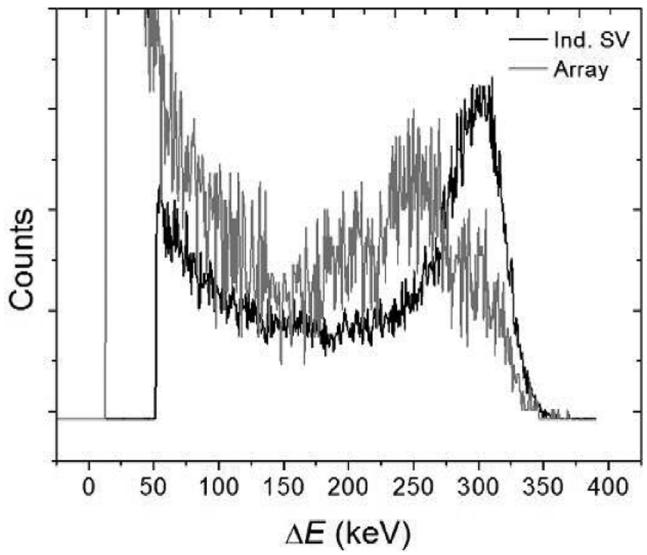

Fig. 10. A comparison of the spectra produced in response to a beam of 3 MeV He ions by a 9 V reverse biased independently read out 2 μm radial width SV and a 10 V reverse biased section of the array. The significantly most significant energy in the spectrum produced by the array is lower than the corresponding energy in the spectrum produced by the independent SV.

presented above. While both spectra have a pronounced peak in the region of 230–330 keV, the peaks do not line up and the array spectrum appears to have a smaller unresolved peak of higher energy next to it. To investigate this phenomenon IBIC frequency distribution maps were generated to examine the spatial origin of the events that contributed to regions of interest on the spectrum. Fig. 11 shows frequency distribution maps for the regions: a) 0–160 keV, b) 160–220 keV, c) 220–270 keV and d) 270–360 keV. From Fig. 11(a) it is possible to see that low energy events (0–160 keV) are due to the collection of diffused charge that occurs when ions are incident upon the periphery of each SV. The square geometry of the mesa structure is observed in this array scan, and not the individual SV scan, due to the inclusion of events with an energy of less than 45 keV. During the scan of the individual SV the MCA threshold was set at $\sim$50 keV. The frequency distribution map in Fig. 11(b) presents the spatial origin of events up to an energy of 220 keV. This energy region is similar to that of the frequency distribution map in Fig. 8(a). Both maps show comparable charge collection

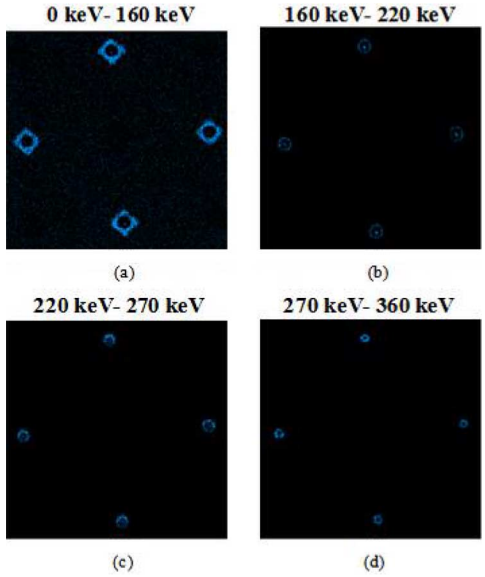

Fig. 11. (a)–(d) Event frequency distribution maps corresponding to the 4 distinct regions of the energy spectrum in Fig. 10. In (c) a high frequency of counts is observed on the upper side of the SV due to the asymmetry of the fabrication mask used to create the fragment of the array. This leads to a statistically more significant number of counts in the region of the spectrum just below the full energy peak.

characteristics. This further confirms the similarity of a singularly produced SV and a SV produced as part of an array.

Close examination of the IBIC maps in Figs. 9 and 11(b) reveals that the n^+ core of each SV in the array is not concentric with the outer p^+ region of the SV. This is most likely the result of a mismatch between masks during the fabrication process. The mismatch has led to a slight loss of radial symmetry in the electric field distribution throughout the SV and subsequent non uniform charge collection characteristics. This explains the difference in the deposited energy spectrum of the array as compared to the single SV (Fig. 10). The steep gradient of the $1/r$ electric field away from the n^+ core has resulted in a region of weak electric field to one side of the SV. Ions incident in this region give rise to the events seen in the main peak of the array spectrum as shown in the frequency distribution map of Fig. 11(c). The map in Fig. 11(d) shows full charge collection is occurring within close proximity to the n^+ core where the electric field is strong. The energy of charge collected in this region is equal to the energy of the main peak in the individual SV spectrum. Thus with an improved matching of masks during the fabrication process the spectrum produced by an array should be in good agreement with the spectrum produced by a single SV.

Results from this IBIC investigation have demonstrated the feasibility of a full array of cylindrical SVs. Results have also demonstrated the excellent spatial resolution IBIC is capable of for micron sized structures and its capability for application in the quality assurance of modern radiation detector fabrication processes.

IV. Conclusion

A SOI microdosimeter with a novel array of 3D cylindrical SVs was introduced and investigated. The design of this micro-

dosimeter addressed the issues identified as limiting the performance of a previous SOI microdosimeter technology. An IBIC study has shown that each individual prototype concentric *p-i-n* diode structure performs as a well defined 3D cylindrical site of near 100% charge collection efficiency, corresponding to a truly micron sized SV, and an array of these SVs can be successfully read out in a parallel mode. Once a full array has been successfully fabricated this SOI design will have great potential for application in regional microdosimetry.

REFERENCES

[1] H. H. Rossi and M. Zaider, *Microdosimetry and its Applications*. London, U.K.: Springer, 1996.

[2] A. Wroe, A. Rosenfeld, and R. Schulte, "Out-of-Field dose equivalents delivered by proton therapy of prostate cancer," *Med. Phys.*, vol. 34, no. 9, pp. 3449–3456, 2007.

[3] G. Coutrakon *et al.*, "Microdosimetry spectra of the loma linda proton beam and relative biological effectiveness comparisons," *Med. Phys.*, vol. 24, no. 9, pp. 1499–1506, 1997.

[4] Y. Kase *et al.*, "Microdosimetric measurements and estimation of human cell survival for heavy-ion beams," *Radiat. Res.*, vol. 166, pp. 629–638, 2006.

[5] A. Wambersie, P. Pihet, and H. G. Menzel, "The role of microdosimetry in radiotherapy," *Radiat. Protect. Dosim.*, vol. 31, pp. 421–432, 1990.

[6] D. J. Brenner and M. Zaider, "Estimating RBEs at clinical doses from microdosimetric spectra," *Med. Phys.*, vol. 25, no. 6, pp. 1055–1057, 1998.

[7] A. Wambersie, "Contribution of microdosimetry to the specification of neutron beam quality for the choice of 'Clinical RBE' in fast neutron therapy," *Radiat. Protect. Dosim.*, vol. 52, pp. 453–460, 1994.

[8] J. Barak, "Analytical microdosimetry model for proton-induced SEU in modern devices," *IEEE Trans. Nucl. Sci.*, vol. 48, no. 6, pp. 1937–1945, Dec. 2001.

[9] A. J. Wroe *et al.*, "Solid state microdosimetry with heavy ions for space applications," *IEEE Trans. Nucl. Sci.*, vol. 54, no. 6, pp. 2264–2271, Dec. 2007.

[10] D. A. Prokopovich, M. I. Reinhard, I. M. Cornelius, and A. B. Rosenfeld, "SOI microdosimetry for mixed field radiation protection," *Radiat. Meas.*, vol. 43, pp. 1054–1058, 2008.

[11] Microdosimetry, ICRU Rep. 36, Bethesda, MD, 1983.

[12] P. D. Bradley, A. B. Rosenfeld, and M. Zaider, "Solid state microdosimetry," *Nucl. Instrum. Methods Phys. Res. B*, vol. B184, pp. 135–157, 2001.

[13] A. M. Kellerer, "Event simultaneity in cavities. Theory of the distortions of energy deposition in proportional counters," in *Radiat. Res.*, 1971, vol. 48, pp. 216–233.

[14] P. J. McNulty, D. R. Roth, E. G. Stassinopoulos, and W. J. Stapor, T. Dombeck, V. Kelly, and G. P. Yost, Eds., "Characterizing complex radiation environments using more (monitor of radiation effects)," in *Proc. Symp. Detector Research and Development SSC*, Singapore, 1990, pp. 690–692.

[15] J. F. Dicello, H. I. Amols, M. Zaider, and G. Tripard, "A comparison of microdosimetric measurements with spherical proportional counters and solid state detectors," *Radiat. Res.*, vol. 82, pp. 441–453, 1980.

[16] P. J. McNulty, D. R. Roth, E. G. Stassinopoulos, and W. J. Stapor, T. Dombeck, V. Kelly, and G. P. Yost, Eds., "Characterizing complex radiation environments using MORE(monitor of radiation effects)," in *Proc. Symp. Detector Research and Development., SSC World Scientific*, 1990.

[17] D. R. Roth, P. J. McNulty, W. J. Beauvais, R. A. Read, and E. G. Stassinopoulos, "Solid-state microdosimeter for radiation monitoring in spacecraft and avionics," *IEEE Trans. Nucl. Sci.*, vol. 41, no. 6, pp. 2118–2124, Dec. 1994.

[18] L. Z. Scheick, B. Blake, and P. J. McNulty, "Microdosimetry of the ultraviolet erasable programmable read-only memory experiment on the microelectronics and photonics test bed: recent advances in small-volume analysis," *IEEE Trans. Nucl. Sci.*, vol. 52, no. 6, pp. 2300–2306, Dec. 2005.

[19] S. Agosteo *et al.*, "A feasability study of a solid-state microdosimeter," *Appl. Radiat. Isot.*, vol. 63, pp. 529–535, 2005.

[20] A. B. Rosenfeld, P. D. Bradley, I. Cornelius, and J. Flanz, "A new silicon detector for microdosimetry applications in proton therapy," *IEEE Trans on Nucl. Sci.*, vol. 47, no. 4, pp. 1386–1394, Aug. 2000.

[21] P. D. Bradley, "The Development of a Novel Silicon Microdosimeter for High LET Radiation Therapy," Ph.D. dissertation, Dept. Engineering Physics, Univ. Wollongong, Wollongong, Australia, 2000.

[22] P. D. Bradley and E. Normand, "Single event upsets in implantable cardioverter defibrillators," *IEEE Trans. Nuc. Sci.*, vol. 45, no. 6, pp. 2929–2940, Dec. 1998.

[23] S. Pepper, M. Farnitano, J. C. J. Hazeltine, and D. Bailey, Lessons Learned in Testing of Safeguards Equipment IAEA Rep., IAEA-SM-367/7/03.

[24] J. L. Leray, "Effects of atmospheric neutrons on devices, at sea level and in avionics embedded systems," *Microelectron. Reliab.*, vol. 47, pp. 1827–1835, 2007.

[25] P. D. Bradley, A. Rosenfeld, B. Allen, J. Coderre, and J. Capala, "Performance of silicon microdosimetry detectors in boron neutron capture therapy," *Radiat. Res.*, vol. 151, pp. 235–243, 1999.

[26] I. Cornelius and A. Rosenfeld, "Verification of Monte Carlo calculations in fast neutron therapy using silicon microdosimetry," *IEEE Trans. Nucl. Sci*, vol. 51, no. 3, pp. 873–877, Jun. 2004.

[27] I. M. Cornelius, A. B. Rosenfeld, R. Seigele, and D. Cohen, "LET dependence of the charge collection efficiency of silicon microdosimeters," *IEEE Trans. Nucl. Sci*, vol. 50, no. 6, pp. 2373–2379, Dec. 2003.

[28] A. B. Rosenfeld, P. D. Bradley, I. Cornelius, B. J. Allen, M. Zaider, R. L. Maughan, J. C. Yanch, J. Coderre, J. B. Flanz, and T. Kobayashi, "Solid state microdosimetry in hadron therapy," *Radiat. Protect. Dosim.*, vol. 101, pp. 431–434, 2002.

[29] M. Reinhard *et al.*, "Response of a SOI microdosimeter to a 238PuBe neutron source," in *Proc. IEEE NSS Conf. Rec.*, Oct. 2005, vol. 1, pp. 68–72.

[30] P. D. Bradley, A. B. Rosenfeld, K. K. Lee, D. N. Jamieson, G. Heiser, and S. Satoh, "Charge collection and radiation hardness of a SOI microdosimeter for medical and space applications," *IEEE Trans Nucl. Sci.*, vol. 45, no. 6, pp. 2700–2010, Dec. 1998.

[31] W. H. Lim *et al.*, "Cylindrical-On-Insulator microdosimeter: Design, fabrication and TCAD modelling," in *Proc. IEEE NSS/MIC Conf.*, Honolulu, HI, 2007.

[32] I. Cornelius *et al.*, "Ion beam induced charge characterisation of a silicon microdosimeter using a heavy ion microprobe," *Nucl. Instrum. Methods Phys. Res. B*, vol. B190, pp. 335–338, 2002.

[33] NIST A-Star Database [Online]. Available: http://physics.nist.gov/PhysRefData/Star/Text/ASTAR.html